Complex Dynamics of Droplet Traffic in a Bifurcating Microfluidic Channel: Periodicity, Multistability, and Selection Rules

D. A. Sessoms, A. Amon, L. Courbin, and P. Panizza
IPR, UMR CNRS 6251, Campus Beaulieu, Université Rennes 1, 35042 Rennes, France
(Received 22 December 2009; published 5 October 2010)

The binary path selection of droplets reaching a T junction is regulated by time-delayed feedback and nonlinear couplings. Such mechanisms result in complex dynamics of droplet partitioning: numerous discrete bifurcations between periodic regimes are observed. We introduce a model based on an approximation that makes this problem tractable. This allows us to derive analytical formulae that predict the occurrence of the bifurcations between consecutive regimes, establish selection rules for the period of a regime, and describe the evolutions of the period and complexity of droplet pattern in a cycle with the key parameters of the system. We discuss the validity and limitations of our model which describes semiquantitatively both numerical simulations and microfluidic experiments.

DOI: 10.1103/PhysRevLett.105.154501 PACS numbers: 47.61.−k, 47.20.Ky, 47.55.D−, 47.60.Dx

Understanding the flow of discrete elements through networks is of importance for diverse phenomena, including microfluidics for controlled droplet traffic [1], blood flows for functioning cardiovascular systems [2], and even road traffic for optimized road networks [3]. Addressing this issue requires a description of the mechanisms that govern flow partitioning at a node. In most cases, splitting rules are complex since they often involve either human decision-making or noise [2,4]. Droplet traffic thus appears as a model system since a droplet reaching a node simply flows in the arm having the largest volumetric flow rate [5]. Despite this robust and simple rule, this paradigmatic system exhibits complex dynamics, also observed in cellular automata [6], resulting from iterations of simple rules and time-delayed feedback [7–11]. The presence of droplets in a channel modifies its hydrodynamic resistance so that the path selection of a droplet at a node is affected by the trajectories of the previous ones. This yields periodic patterns that are common to any traffic flow. The widely studied situation of a droplet flowing through a loop leads to the emergence of a wealth of bifurcations between different periodical partitioning regimes with discrete periods and aperiodical regimes [7–11]. Even in this simple configuration, an understanding of the physical parameters and relations that completely describe the dynamical response has remained elusive or limited to specific configurations.

Here we introduce an approximation that allows the theoretical description of the complex dynamics of droplet traffic through a loop. Using this working hypothesis, we derive analytical formulae that (i) predict the occurrence of the bifurcations between consecutive periodical regimes, (ii) establish selection rules for the period of a regime, and (iii) describe the evolutions of the period and complexity of droplet pattern in a cycle with the key parameters of the system. These predictions capture the main features of numerical simulations [7,9,11]. Our findings also underline the crucial role of natural noise, intrinsic in experiments, in evidencing multistability between periodic states. Indeed, our microfluidic experiments can be rationalized when natural noise (i.e., stochastic shifts of the droplet position or size) is introduced in our model.

We consider a periodic train of droplets reaching the inlet node of an asymmetric loop having two arms of different lengths L_1 and L_2 with $\Lambda = L_2/L_1 > 1$ [Fig. 1(a)]. The monodisperse droplets emitted at a constant period τ flow at a velocity $v = \frac{\lambda}{\tau}$, where λ is the distance separating two droplets. At the inlet node, a droplet flows into the arm having the lower hydrodynamic resistance. When λ is larger than a value λ_f, all droplets flow into the shorter arm; the device acts as a filter [4]. As λ decreases, the droplets which flow into the short arm may increase its hydrodynamic resistance sufficiently so that it eventually overcomes that of the long arm. When $\lambda < \lambda_f$, partitioning of the droplets between the two arms is observed so that the hydrodynamic resistances of the two arms remain nearly equal in the steady state. In this regime, the binary ''choice'' made by each droplet modifies the instantaneous hydrodynamic resistance of the ith arm in which it flows ($\propto L_i + N_i L_d$) and consequently affects the path selection of the following droplets; N_i is the number of droplets present in the ith arm, and the length L_d corresponds to the excess hydrodynamic resistance per drop. This collective time-delayed feedback mechanism [7–11], for which delays are related to the retention times of the droplets in the loop, yields the complex dynamics that we aim to understand.

Analyzing these dynamics is challenging because of the nonlinear nature of the time delays due to the coupling between N_i and v_i, the droplet velocities in arm (i) [12], and the splitting rules. In the repartition regime, the mean droplet velocity in each arm in the steady state $\langle v_i \rangle$ is nearly $\frac{v}{2}$ [10]. In this Letter, we assume that v_i is constant and equal to $\frac{v}{2}$. This ''mean-field'' approximation makes

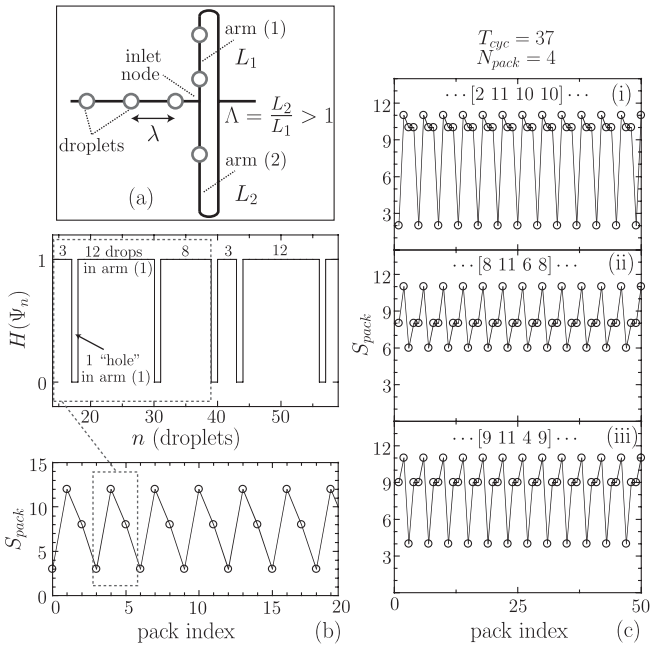

FIG. 1. (a) Schematic of the flow model defining λ, L_1, $L_2 > L_1$, and Λ. (b) Top panel: Typical evolution of the numerical binary signal $H(\Psi_n)$ with the droplet number n. Each 1 and 0, respectively, stand for one droplet flowing in arm (1) and one hole present in arm (1) [i.e., one droplet flowing in arm (2)]. Bottom panel: $H(\Psi_n)$ is processed into a sequence of packs of droplets, S_{pack}. (c) For given values of $L_d = 2.7$, $\lambda = 8.2$, $L_1 = 100$, and $L_2 = 150$, S_{pack} strongly depends on initial conditions: the arm (2) is initially empty and the arm (1) is filled with droplets located at positions x_k, where $k \geq 1$ is an integer: (i) $x_k = kL_1/20$, (ii) $x_k = kL_1/10$, and (iii) $x_k = kL_1/5$.

the problem tractable and is justified when working within the limit $L_d \ll L_i + N_i L_d$, for which the variations of v_i, due to the entrance or exit of a droplet in the loop, is small ($\sim 1\%$ in our study).

Using this approximation, we begin by deriving the algorithm that governs the flow, building on earlier works [7,9,10]. The time is discretized in τ units and, as velocities are constant, space is also discretized: possible droplet positions in the loop are multiple of $\lambda/2$, which yields a finite number of possible configurations. Moreover, since our model is deterministic, only periodic outcomes are expected. Partitioning occurs such that a droplet flows into the arm having the smaller hydrodynamic resistance, and we code the resulting binary choices into series of 1 (one droplet flows in the short arm) and 0 (one droplet flows in the long arm, i.e., a "hole" flows in the short arm) [Fig. 1(b)]. This can be written as $H(\Psi_n)$ where H is the Heaviside function and $\Psi_n = (L_2 - L_1)/L_d + N_2(n) - N_1(n)$ represents the normalized difference of the hydrodynamic resistance between both arms at time n. Our procedure consists of three steps: (1) before the injection of each droplet at the node, we first compute the number of droplets present in each arms and the resulting value of Ψ_n, (2) we determine the path taken by the incoming droplet, (3) we move all the droplets by intervals of $\lambda/2$ along each arms, with one or more droplets possibly exiting the loop. All droplets flowing through arm (i) share the same retention time $T_i^\star = \frac{2L_i}{\lambda}$, yielding the discrete time $T_i = \text{ceil}(\frac{2L_i}{\lambda})$ used in our iterative analysis. The values of Ψ_n and N_i are determined in steps (1) and (2), respectively. $N_1(n)$ and $N_2(n)$ are given by:

$$N_i(n) = \sum_{k=n-T_i+1}^{n} H(\epsilon_i \Psi_k),$$

$$\text{where } \epsilon_1 = 1 \quad \text{and} \quad \epsilon_2 = -1.$$

The binary signal $H(\Psi_n)$ is then processed into a series of "packs," S_{pack}, a pack being the number of droplets flowing through the shorter arm between two successive droplets taking the longer arm (including $S_{\text{pack}} = 0$, if two subsequent droplets flow through the longer arm) [Fig. 1(b)]. As expected, Fig. 1(b) shows the emergence of periodicity. Although the composition of the packs during one cycle shows a strong dependence on initial conditions [Fig. 1(c)], the number of droplets N_{cyc}, i.e., the cycle time $T_{\text{cyc}} = N_{\text{cyc}}$, and packs per cycle, N_{pack}, are two invariants. We next derive mathematical expressions for these invariants.

Because of the discrete nature of the system and feedbacks, the difference $N_1 - N_2$ is either $\text{floor}(\frac{L_2-L_1}{L_d})$ or $\text{ceil}(\frac{L_2-L_1}{L_d})$, so that the difference of the hydrodynamic resistances remains the closest to 0 in L_d units. When the total number of droplets $N_1 + N_2$ is constant, it can be shown that N_1 and N_2 are both constant and that the cycle time is $T_2 - T_1$; the conservation of the dispersed phase is then verified at each time τ. However, $N_1 + N_2$ is usually not constant but takes only two consecutive values: either N_1 is constant and N_2 fluctuates by 1 ($T_{\text{cyc}} = T_1$) or N_2 is constant and N_1 fluctuates by 1 ($T_{\text{cyc}} = T_2$).

Bifurcations from one periodical regime to another are controlled by λ (see the raw numerical data in Ref. [13]). The first bifurcation occurs at the filter-repartition transition, when the hydrodynamic resistance of the short arm full of droplets becomes larger than that of the empty long one, i.e. $\frac{L_2-L_1}{L_d} < \text{floor}(\frac{2L_1}{\lambda})$; hence, $\lambda_f = \frac{2L_1}{\text{floor}(\frac{L_2-L_1}{L_d})+1}$. Decreasing λ further allows a remaining number of droplets $M = \text{ceil}(\frac{2L_1}{\lambda}) - \text{floor}(\frac{L_2-L_1}{L_d})$ to be shared between the two outlets to nearly equalize their hydrodynamic resistances. Denoting N_1^H the number of holes in the short arm, we directly show that $N_2 + N_1^H$ can take only two values, M or $M - 1$. When $T_{\text{cyc}} = T_1$, N_1^H is constant and $N_2 = M - N_1^H - 1$ during a time $t < T_1$ and $M - N_1^H$ during $T_1 - t$. Because of the conservation of the total number of droplets in the two arms, $(T_1 - t)(M - N_1^H) + t(M - N_1^H - 1) = T_2 N_1^H$. Using a similar analysis when T_{cyc} is equal to T_2 and $T_2 - T_1$, we obtain that the following condition must be fulfilled for $i = 1$ or 2:

$$0 \leq \frac{T_i}{T_1+T_2}M - N_i^{(H)} \leq \frac{T_i}{T_1+T_2}. \quad (1)$$

Using Eq. (1), the two invariants, $T_{\rm cyc}$ and $N_{\rm pack}$, can be predicted for a given value of λ. We calculate the fractional parts ϵ_p of pM and ϵ_q of qM, with $p = \frac{T_1}{T_1+T_2}$ and $q = \frac{T_2}{T_1+T_2} = 1-p$. Noting that $\epsilon_p + \epsilon_q$ must be equal to 0 or 1, we determine four possible cases: (i) $\epsilon_p = \epsilon_q = 0$, (ii) $\epsilon_p = p$ and $\epsilon_q = q$, (iii) $0 < \epsilon_p < p$ and $q < \epsilon_q < 1$, (iv) $p < \epsilon_p < 1$ and $0 < \epsilon_q < q$.

In case (i), pM and qM are integers, N_1^H and N_2 are then simultaneously constant and respectively given by those integers; $T_{\rm cyc} = T_2 - T_1$ and $N_{\rm pack} = N_2 - N_1^H = (q-p)M$. In case (ii), $p(M-1)$ and $q(M-1)$ are integers and, respectively, set the values of N_1^H and N_2 which are both constant: $T_{\rm cyc} = T_2 - T_1$ and $N_{\rm pack} = (q-p)\times(M-1)$. In cases (iii) and (iv), the condition given in Eq. (1) is no longer fulfilled for both $i = 1$ and 2: N_1^H and N_2 cannot be simultaneously constant. In case (iii), N_1^H is constant and equal to the integer part of pM, $T_{\rm cyc} = T_1$ and $N_{\rm pack} = N_1^H$. In case (iv), N_2 is constant and equal to the integer part of qM, $T_{\rm cyc} = T_2$ and $N_{\rm pack} = N_2$. As expected, these selection rules mirror our numerical simulations that assume a constant droplet velocity in both arms [13]. Successive bifurcations are related to a variation of 1 in either T_1 or T_2, and are expected to occur when the residence times $T_i^\star = \frac{2L_i}{\lambda}$ take integer values. This happens for specific values of $\lambda = \lambda_c(i,k)$:

$$\frac{2L_i}{\lambda_c(i,k)} = \text{floor}\left(\frac{L_2-L_1}{L_d}\right) + k, \quad (2)$$

where $k \in \mathbb{N}^\star$ and $i = 1, 2$.

We next compare our predictions with the full-model numerical simulations, i.e., performed with nonlinear couplings between v_i and N_i [7,9,10]. As shown in Fig. 2, although our approximation that neglects velocity fluctuations in the loop may seem severe, our simplified model quantitatively captures most features of the numerical data. As predicted, we obtain numerous periodic regimes whose periods, $T_{\rm cyc}$, are discrete and correspond to either T_1, T_2, or $T_2 - T_1$. Each of these regimes, or "plateaus," exists over a large range of the parameter λ. Our simple model describes well the occurrence of the bifurcations between two consecutive plateaus and the period selection for a given one. In addition, the explicit equation, Eq. (2), predicts well the positions of these bifurcations. We observe, however, small shifts of the position of the bifurcations that do not alter the global picture, and periodic regimes with unusually long cycle times emerging between two successive plateaus. Since these singular regimes that are not predicted by our model exist only for a very narrow range of the parameter λ, narrower than the experimental stochastic noise of λ as discussed below, they are not observable experimentally which makes them irrelevant to our experiments. As shown in [13] where we provide a more quantitative comparison of both the models, similar behaviors are obtained for the evolution of $N_{\rm pack}$ with λ/λ_f.

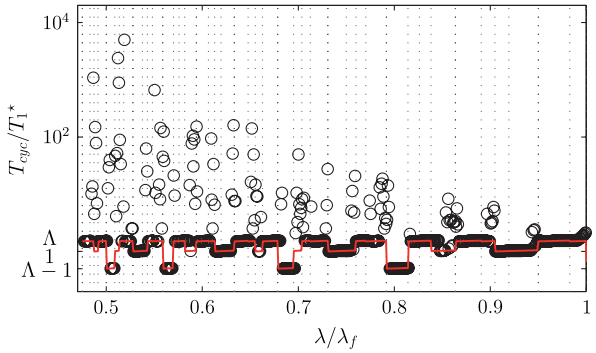

FIG. 2 (color online). Numerical simulations performed with velocity fluctuations: Bifurcation diagrams of $T_{\rm cyc}/T_1^\star$ with λ/λ_f. The vertical lines are predictions calculated using Eq. (2) and the red line corresponds to the selection rules derived in the text. $L_d = 2.7$, $L_1 = 100$, and $L_2 = 150$.

To further validate our model, we carry out the following experiments. We use a microfluidic device [Fig. 3(a)] having an asymmetric loop with two arms of different lengths $L_1 < L_2$ but same cross-section, and we study the traffic of trains of monodisperse droplets (for details about the experimental system, see Ref. [10]). We control the droplet size r by adjusting the water and oil flow rates, and the distance λ by using the dilution module [Fig. 3(a)]; λ is

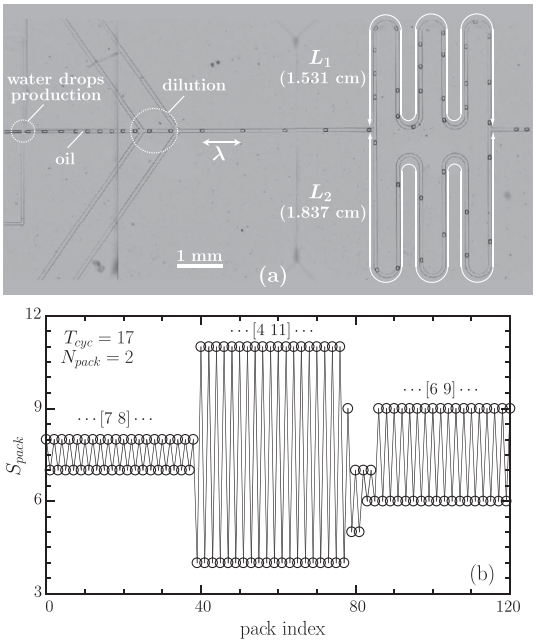

FIG. 3. (a) Experimental setup: shown are the water-in-oil droplet production stage, the dilution module, and the asymmetric loop. (b) Typical variation of $S_{\rm pack}$. The dynamical response is complex, yet $T_{\rm cyc}$ and $N_{\rm pack}$ are conserved during this long time series.

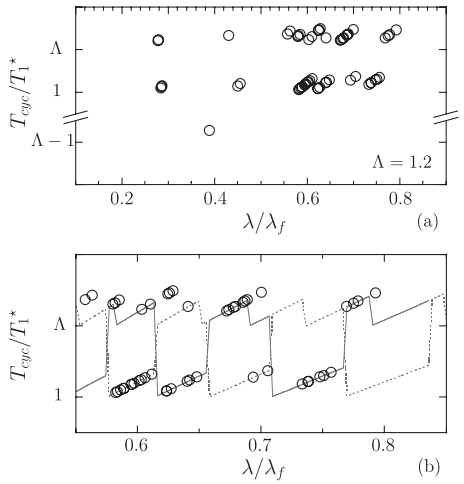

FIG. 4. (a) Experimental bifurcation diagrams of $T_{\rm cyc}/T_1^\star$ as a function of λ/λ_f: the three branches correspond to $T_{\rm cyc}$ equal to T_2, to T_1, and to $T_2 - T_1$. (b) Magnification for $\lambda/\lambda_f = 0.55$–0.85 showing the strong dependence of the bifurcations on the excess length L_d. The two grey lines stand for predictions computed using two values of L_d: (solid) $L_d = 305$ μm, (dashed) $L_d = 331$ μm.

maintained large enough so that droplets do not interact. We use a high-speed camera (frame rate $\sim$1000 frames/s) to monitor droplet traffic, and we analyze the movies with custom-written MATLAB software to determine the series of binary choices between the short and long arm, coded respectively by 1 and 0 similarly to the simulations. An important feature of our experiments is that L_1 and L_2 are chosen large enough so that experiments are performed within the limit that we explored numerically, i.e. $L_d \ll L_i + N_i L_d$ [10].

When $\lambda < \lambda_f$, the signal of the packs exhibits complex dynamics, as shown by a succession of different periodical behaviors lasting hundreds of droplets [Fig. 3(b)]. Although the underlying patterns of droplet partitioning change, Fig. 3(b) shows that those successive periodic regimes share the same periodicity $T_{\rm cyc}$ and the number of packs $N_{\rm pack}$. We next study the variations of these invariants with λ. In agreement with our analytical predictions, when λ decreases, $T_{\rm cyc}$ and $N_{\rm pack}$ both increase, leading to increasing complexity of the droplet repartition pattern for a given periodic regime (not shown here). We present in Fig. 4 the evolution of $T_{\rm cyc}/T_1^\star$ with λ/λ_f. We obtain numerous discrete bifurcations between three distinct branches which, as expected by our model, correspond to $T_{\rm cyc} = T_i$ and to $T_{\rm cyc} = T_2 - T_1$ [Fig. 4(a)]. By adjusting the value of L_d, our set of experiments concurs with predictions, as shown in [Fig. 4(b)].

Figure 1(c) shows that the pack composition presents a strong dependence on initial conditions. Such coexistence of several attractors for a set of parameters, called multistability, is a common feature for many delay systems, e.g., models of neurons [14]. The dynamics can then commute from one regime to another when some noise leads the system to quit the basin of attraction of one attractor to reach another [11]. The presence of noise can be implemented in our numerical simulations by including fluctuations of λ or L_d, which are indeed inherent to experiments ($\sim 2\%$, [15]), to reproduce a complex dynamical response as that of Fig. 3(b) (not shown here).

In closing, we observe multistability between different periodic states in an asymmetric microfluidic device. The simplicity of our model system makes it a promising experimental and theoretical tool to understand dynamics in delayed feedback systems. Our results provide a robust way to understand and control droplet traffic complex dynamics by applying the selection rules we identified. Our system, discretized both in space and time and controlled by simple iterative rules, also illustrates digital microfluidics as a simple example of cellular automaton [6].

D. A. Sessoms acknowledges support from the Swiss NSF Grant No. PB FR-120924. We thank A. Ajdari for fruitful discussions, and an anonymous referee for helpful feedback.

[1] H. A. Stone, A. D. Stroock, and A. Ajdari, Annu. Rev. Fluid Mech. **36**, 381 (2004).
[2] R. T. Carr and M. Lacoin, Ann. Biomed. Eng. **28**, 641 (2000).
[3] K. Nagel, Phys. Rev. E **53**, 4655 (1996).
[4] M. Belloul, W. Engl, A. Colin, P. Panizza, and A. Ajdari, Phys. Rev. Lett. **102**, 194502 (2009).
[5] W. Engl, M. Roche, A. Colin, P. Panizza, and A. Ajdari, Phys. Rev. Lett. **95**, 208304 (2005).
[6] S. A. Kauffman, Physica (Amsterdam) **10D** , 145 (1984).
[7] F. Jousse, R. Farr, D. R. Link, M. J. Fuerstman, and P. Garstecki, Phys. Rev. E **74**, 036311 (2006).
[8] M. J. Fuerstman, P. Garstecki, and G. M. Whitesides, Science **315**, 828 (2007).
[9] M. Schindler and A. Ajdari, Phys. Rev. Lett. **100**, 044501 (2008).
[10] D. A. Sessoms, M. Belloul, W. Engl, M. Roche, L. Courbin, and P. Panizza, Phys. Rev. E **80**, 016317 (2009).
[11] O. Cybulski and P. Garstecki, Lab Chip **10**, 484 (2010).
[12] The droplet velocity in arm i is $v_i = (1 - \frac{L_i + N_i L_d}{L})v$, where $L = L_1 + L_2 + (N_1 + N_2)L_d$. For details, see [10].
[13] See supplementary material at http://link.aps.org/supplemental/10.1103/PhysRevLett.105.154501.
[14] J. Foss, A. Longtin, B. Mensour, and J. Milton, Phys. Rev. Lett. **76**, 708 (1996).
[15] Experiments show that L_d is a strong function of r [4]; i.e., fluctuations of L_d are related to those of r.